

**Pinch and swell structures**

R. Gardner et al.

This discussion paper is/has been under review for the journal Solid Earth (SE).  
Please refer to the corresponding final paper in SE if available.

# Pinch and swell structures: evidence for brittle-viscous behaviour in the middle crust

**R. Gardner, S. Piazzolo, and N. Daczko**

Australian Research Council Centre of Excellence for Core to Crust Fluid Systems/GEMOC,  
Department of Earth and Planetary Sciences, Macquarie University, Sydney, NSW 2109,  
Australia

Received: 25 March 2015 – Accepted: 27 March 2015 – Published: 24 April 2015

Correspondence to: R. Gardner (robyn.gardner@mq.edu.au)

Published by Copernicus Publications on behalf of the European Geosciences Union.

Title Page

Abstract

Introduction

Conclusions

References

Tables

Figures



Back

Close

Full Screen / Esc

Printer-friendly Version

Interactive Discussion



## Abstract

The flow properties of middle to lower crustal rocks are commonly represented by viscous flow. However, examples of pinch and swell structures found in a mid-crustal high strain zone at St. Anne Point (Fiordland, New Zealand) suggest pinch and swell structures are initiated by brittle failure of the more competent layer in conjunction with material softening. On this basis we develop a flexible numerical model using brittle-viscous flow where Mohr–Coulomb failure is utilised to initiate pinch and swell structure development. Results show that pinch and swell structures develop in a competent layer in both Newtonian and non-Newtonian flow provided the competent layer has enough viscosity contrast and initially fails brittly. The degree of material softening after initial failure is shown to impact pinch and swell characteristics with high rates of material softening causing the formation of thick necks between swells by limiting the successful localisation of strain. The flow regime and yielding characteristics of the matrix do not impact pinch and swell structure formation itself, so long as the matrix is less competent. To aid analysis of the structures and help derive the flow properties of rocks in the field, we define three stages of pinch and swell development and offer suggestions for measurements to be made in the field.

Our study suggests that Mohr–Coulomb behaviour combined with viscous flow is an appropriate way to represent the heterogeneous rocks of the middle to lower crust. This type of mid-crustal rheological behaviour has significant influence on the localization of strain at all scales. For example, inclusion of Mohr–Coulomb brittle failure with viscous flow in just some mid-crustal layers within a crustal scale model will result in strain localisation throughout the whole crustal section allowing the development of through-going high strain structures from the upper crust into the middle and lower crust. This localization then has a significant effect on developing near-surface structures.

SED

7, 1517–1554, 2015

## Pinch and swell structures

R. Gardner et al.

Title Page

Abstract

Introduction

Conclusions

References

Tables

Figures



Back

Close

Full Screen / Esc

Printer-friendly Version

Interactive Discussion



# 1 Introduction

Rock deformation in the Earth's crust is known to be highly heterogeneous (Rudnick and Gao, 2003; Taylor and McLennan, 1985) with localized domains of high strain seen in metamorphic zones from the upper to lower continental crust. For example, the proto-Darling Fault which defines the edge of the Yilgarn craton in Western Australia has three structural zones and reaches to 40 km depth (Middleton et al., 1993). Crustal scale numerical models of tectonic processes using rheological flow properties have provided important insights into scenarios such as continental break-up and collision, and their surface expression in the current landscape. However, these models do not explain the occurrence of these deeply penetrating crustal scale zones of strain localisation. While there is ongoing discussion of appropriate rheological models for the upper crust (e.g. Moresi and Mühlhaus, 2006), it is generally accepted that the most suitable rheological model for the middle to lower crust is thermally activated viscous flow (e.g. Molnar and Houseman, 2004). However, there is strong field evidence for brittle fracturing in the middle to lower continental crust (e.g. Brander et al., 2012; Fusesis et al., 2006; Guermani and Pennacchioni, 1998; Mancktelow and Pennacchioni, 2005; Segall and Simpson, 1986, 1985) suggesting that this fundamental assumption may be flawed.

For decades geologists have used field evidence of different structures to derive the flow characteristics of middle to lower crustal rocks. For example, Treagus and Treagus (2002) used deformed pebbles, Ramsay (1980) used shear zones while boudins and mullions have been used in several studies (e.g. Kenis et al., 2004; Urai et al., 2001). Boudins (from French *boudin*, "sausage") are chains of rock fragments sometimes joined by thin necks giving them the appearance of a string of sausages (Lohest et al., 1908; Ramsay, 1866). They form when a more competent layer is extended in a weaker matrix, from microscopic to outcrop to regional scales (Goldstein, 1988; Klepeis et al., 1999; St-Onge et al., 2009). Boudins have been used to suggest that the rock units deformed by a mixture of brittle and/or semi-brittle to ductile flow (Abe

## SED

7, 1517–1554, 2015

### Pinch and swell structures

R. Gardner et al.

Title Page

Abstract

Introduction

Conclusions

References

Tables

Figures



Back

Close

Full Screen / Esc

Printer-friendly Version

Interactive Discussion



and Urai, 2012; Arslan et al., 2008; Komoróczy et al., 2013; Marques et al., 2012; van der Molen, 1985). Pinch and swell structures, also called drawn or necked boudins, are a subset of boudins that retain continuity of the drawn layers (Fig. 1a and b). These pinch and swell structures have been reported from a large variety of tectonic settings and crustal levels (Arslan et al., 2008; Goscombe et al., 2004; Hobbs et al., 2010; Kenis et al., 2004; Ponce et al., 2013; van der Molen, 1985).

Investigations of the flow properties related to pinch and swell formation have encompassed three general areas: (i) theoretical analysis (Emerman and Turcotte, 1984; Smith, 1975, 1977) using pure viscous flow which suggests that non-Newtonian flow and material softening is required for pinch and swell formation, (ii) analogue modelling which generally confirmed the earlier theoretical concepts (Kobberger and Zulauf, 1995; Mengong and Zulauf, 2006; Neurath and Smith, 1982; Zulauf and Zulauf, 2005), and (iii) numerical modelling which has so far also concentrated on forming the pinch and swell structures in pure viscous flow, where an initial irregularity on the competent layer edge or within the layer is allowed to grow and dominate any other irregularities to allow strain to localise, thereby causing the pinch and swell structure to initiate (e.g. Passchier et al., 2005; Schmalholz and Maeder, 2012; Smith, 1977). Abe and Urai (2012) and Komoróczy et al. (2013) have used a model where initial brittle deformation caused by high fluid pressure is used to create 90° fractures (mode I; Koehn et al., 2005; Pollard and Segall, 1987; Scholz, 2002) which initiate the boudin structure followed by viscous flow to allow the structures to develop. This model readily creates torn boudins, a subset of boudins where the separated ends of the competent layer fragments are square.

Once initiated pinch and swell structure development is influenced by the flow properties of all the layers (e.g. Schmalholz and Maeder, 2012; Smith, 1977). Viscous flow is assumed and in its simplest form is described by:

$$\dot{\epsilon} = A\sigma^n, \quad (1)$$

**Pinch and swell structures**

R. Gardner et al.

Title Page

Abstract

Introduction

Conclusions

References

Tables

Figures

◀

▶

◀

▶

Back

Close

Full Screen / Esc

Printer-friendly Version

Interactive Discussion



**Pinch and swell structures**

R. Gardner et al.

Title Page

Abstract

Introduction

Conclusions

References

Tables

Figures



Back

Close

Full Screen / Esc

Printer-friendly Version

Interactive Discussion



where  $\dot{\epsilon}$  is the strain rate,  $\sigma$  is differential stress,  $n$  is the stress exponent and  $A$  is a constant which reflects the material properties at a specific temperature and pressure. Material softening, including processes such as grain size reduction, reactions producing softer minerals, influx of fluids and development of crystallographic preferred orientation (e.g. Passchier and Trouw, 2005) during strain localisation is also an important consideration (Hobbs et al., 2009; Neurath and Smith, 1982, 1977; van der Molen, 1985).

Here we examine field examples of several well exposed chains of pinch and swell structures to determine the prerequisites for a numerical model that allows realistic representation of the initiation and characteristics of pinch and swell structures. At the same time, such a model should represent an appropriate alternative to the commonly used viscous flow model of middle to lower crustal rocks.

Here, we systematically test the impact of (i) stress exponent and brittle failure in the competent layer, (ii) initial viscosity ratio of the competent layer to matrix, (iii) layer dependent stress exponent and brittle behaviour, and (iv) material softening associated with the brittle failure on the formation and evolution of pinch and swell structures. We use our models to derive a scheme of simple field measurements on a pinch and swell outcrop which can provide insights into relative rheological properties of the competent layer and the matrix.

The model is then extended to test the effect of the presence of brittle-viscous deformation in a subset of the middle to lower crust layers. We conduct exploratory tests on a crustal scale model with extension investigating the strain localisation throughout the model and the characteristics of the developing surface structures. Our results highlight the importance of including heterogeneity in terms of Mohr–Coulomb behaviour, material softening and viscosity differences on the dynamics of the developing structures at all scales.

## 2 Pinch and swell structures: field and thin section observations and initial interpretation

The rock platform at St. Anne Point, Fiordland, New Zealand (44°34'19.9" S 167°46'55.3" E) displays an extensive variety of mafic pinch and swell structures, many in long chains developed in a meta-sedimentary matrix (Fig. 1b). Parallel, 2 mm to 50 cm thick mafic layers run SW–NE across the rock platform, generally parallel to the overall steeply dipping foliation of the matrix sedimentary layers. Structures within the mafic layers are variable (Fig. 1), with some layers forming well defined pinch and swell chains (Fig. 1b) and others displaying only minor undulation of the mafic to felsic edge. Very narrow (Fig. 1a) to wide (Fig. 1b) neck thicknesses as well as short to long swell separations are developed (Fig. 1a and b). Numerous examples can be seen of apparently brittle failure within the mafic layers (Fig. 1c), where pinch and swell structures typically have residual evidence of conjugate sets of fractures at 30 to 40° to the foliation (Fig. 1) and general layer orientation. Within the swell structures the internal foliation has been variably deflected, deviating up to 15° from the orientation of the general matrix foliation (Fig. 1c).

Pairs of samples were taken from the swell centre and edge of the mafic competent layer in multiple pinch and swell chains. A summary of microstructural features is provided here (see Supplement for detailed thin section descriptions). The main difference between swell centre and swell edge samples is the relative proportion of phases. The swell centre samples have more amphibole + garnet but less biotite + quartz + plagioclase compared to neck samples. In all samples amphibole grains are fractured, however, such fractures are much more common in swell edges. In all cases, the fractures are filled with quartz, biotite and/or plagioclase (Fig. 1d, e. red arrows). Strain shadows around garnet grains contain the same minerals and indicate fracturing and ductile fabrics formed under similar amphibolite facies conditions (Klepeis et al., 1999). In addition, swell edge samples have smaller grain size and exhibit well developed shear bands.

### Pinch and swell structures

R. Gardner et al.

Title Page

Abstract

Introduction

Conclusions

References

Tables

Figures



Back

Close

Full Screen / Esc

Printer-friendly Version

Interactive Discussion



**Pinch and swell structures**

R. Gardner et al.

Title Page

Abstract

Introduction

Conclusions

References

Tables

Figures



Back

Close

Full Screen / Esc

Printer-friendly Version

Interactive Discussion



Brittle fractures in the centre of the swell (Fig. 1d) are at right angles to the general foliation and are not associated with any shear bands. By contrast, similar to outcrop scale brittle features, shear bands and brittle deformation in swell edge samples are at 30–40° angles to the general foliation, thus representing mode II fractures (Fig. 1e). The presence of numerous fractured grains in swell edges suggests that these fractures may initiate and develop into a through-going shear band (Fig. 1e). These shear bands in turn, are inferred to potentially develop into outcrop scale failures.

The observed assemblage as well as the steeply dipping, SW–NE trending foliation indicate the deformation occurred during the regional  $D_3$  dextral transpression event (Klepeis et al., 1999). This event occurred at upper greenschist to amphibolite facies conditions at  $\sim 8.7$  kbar and  $\sim 585$  °C (Klepeis et al., 1999). These conditions are consistent with amphibole and garnet undergoing brittle deformation (Passchier and Trouw, 2005), while quartz and plagioclase deform in a generally ductile manner (Passchier and Trouw, 2005; Rybacki and Dresen, 2004). The spatial association of increased brittle deformation, presence of hydrous minerals and shear band formation at the swell edge suggests the localisation of strain in the mafic layer occurred at swell necks and is associated with both mode II failure and fluid influx. The latter influx was aided by local porosity and permeability increase due to failure. Existing (quartz, plagioclase) and newly formed phases (quartz, biotite), that do not deform brittly, undergo dislocation creep as evidenced by undulose extinction, subgrains and irregular boundaries (Stipp et al., 2002). Hence, these phases display non-Newtonian flow (e.g. Ranalli, 1997).

### 3 Conceptual model based on field analysis

Ideally, in any model, the pinch and swell structures should initialise and develop with minimum manual specification of the initial location and orientation where strain concentrates to form the necks. The St. Anne Point samples suggest that Mohr–Coulomb mode II brittle failure (Koehn et al., 2005; Pollard and Segall, 1987; Scholz, 2002) is characteristic of the initiation mechanism as this produces the 30–40° conjugate failure

planes seen in the field. At a shear stress defined by the Mohr envelope the material fails on a plane at an angle of  $\pm\theta^\circ$  to the primary stress direction (Fig. 2a) determined by:

$$\tan(2\theta) = 1/\mu, \quad (2)$$

where  $\mu$  is the friction coefficient. Initial cohesion is the value of shear stress on the Mohr envelope for that material where normal stress is zero and is related to the tensile strength of the material (Fig. 2a).

The observed association of (a) brittle failure and (b) shear band development associated with crystal plastic deformation of abundant “softer” phases (biotite, quartz and plagioclase) at swell edges suggest the edges transition from brittle to ductile deformation in agreement with Brander et al. (2012), Fousseis et al. (2006) and Mancktelow (2006). Therefore, material softening occurring after the initial brittle failure needs to be included in the model. This material softening should incorporate both lower viscosity simulating a higher percentage of “soft” phases and lower cohesion simulating a higher degree of fracturing (grey dashed lines, Fig. 2a).

In addition, the St. Anne Point samples display non-Newtonian flow, so both Newtonian and non-Newtonian flow should be included in the model. Based on these observations, conceptually, a numerical model to describe the growth of pinch and swell structures should encompass: (1) no specified geometric perturbation (e.g. sine waves or notches) in the competent layer, (2) ability to deform by brittle failure resulting in conjugate pairs of fault planes that occur dynamically, (3) ability to soften the material to variable degrees after brittle failure has occurred, (4) ability to implement both Newtonian and non-Newtonian viscous flow.

**Pinch and swell structures**

R. Gardner et al.

Title Page

Abstract

Introduction

Conclusions

References

Tables

Figures



Back

Close

Full Screen / Esc

Printer-friendly Version

Interactive Discussion





## 4 Numerical implementation

### 4.1 General model set up

We used the numerical modelling platform Underworld (Moresi et al., 2003, 2007), a 2-D and 3-D simulation package using Lagrangian particle-in-cell finite element methods for modelling large-scale geodynamic processes on geologic time scales to investigate the initiation and evolution of pinch and swell structures.

We implement 2-D models with two different geometries: (i) a three layer model which is the simplest possible geometry, where the central layer (Fig. 2b, layer B) is more competent and (ii) a multi-layer model with a brittle upper layer i.e. upper crust and variably competent layers in the lower parts (layer B) of the model (Fig. 2d). Passive black marker lines are included in each layer to show the movement of pre-existing planar features such as bedding or foliation as the simulation proceeds (Fig. 2b). All simulations use incompressible Uzawa Stokes Flow calculation on an initial  $1 \times 1$  square that is extended horizontally using a non-dimensional velocity of  $-0.5$  on the left hand side and  $+0.5$  on the right hand side to simulate extension. Top and bottom boundaries are fixed. In all experiments the models were run over 200 iterations or steps, to a stretch (s) of 3.2, with each step increasing the stretch as calculated from the elongation of the original  $1 \times 1$  square based on:

$$s = L/L_i, \quad (3)$$

where  $L$  is the length at that step and  $L_i$  is the initial length (Twiss and Moores, 1992). Non-Newtonian flow simulations use a stress exponent of three ( $n = 3$ , Eq. 1) as we consider this to closely represent the flow of naturally occurring rocks (Table S1). All inputs into the models are non-dimensional. This allows for comparison of only relative properties between the layers and between models.

Each layer material has characteristics that combine to give the material constant (A, in Eq. 1) for the flow in that layer. In its simplest form the material constant is dependent on viscosity. Viscosity, however, is known to be dependent on grain size, temperature

Title Page

Abstract

Introduction

Conclusions

References

Tables

Figures



Back

Close

Full Screen / Esc

Printer-friendly Version

Interactive Discussion



and pressure, activation energy and volume, and the presence or absence of melt and/or water (Hirth and Kohlstedt, 2003). In our model, these variables have been incorporated into a single viscosity value ( $\eta$ ): layer B is more competent than the matrix layers A. An initial viscosity ratio ( $R_V$ ) is calculated:

$$R_V = \eta_{Bi} / \eta_{Ai}, \quad (4)$$

where  $\eta_{Bi}$  is the initial viscosity of the competent layer B and  $\eta_{Ai}$  is the initial viscosity of the matrix layers A. The viscosities for both layers will change depending on the strain rate as the non-Newtonian flow simulations progress. By contrast, in the linear ( $n = 1$ ) Newtonian flow simulations the viscosities are constant (per Eq. 1).

Mohr–Coulomb behaviour was included to model brittle failure by using the Underworld implementation of Moresi and Mühlhaus (2006) which optionally incorporates material softening for the particles that have undergone yielding. This provides the capability of a layer behaving in a plastic manner by brittle fracturing then flowing as a viscous fluid. Pressure is not specifically reported here because in this implementation it has an inverse relationship to viscosity (see Eq. (3) in Moresi and Mühlhaus, 2006). Theoretically, as stress is increased, the layers should undergo first, pure elastic deformation at very low strain (cross-hatched and dotted areas in Fig. 2c), followed by viscous deformation (Griggs and Handin, 1960). While elastic behaviour is very important at very low strain of less than 1.03 stretch (e.g. Ranalli, 1997), we simplify the model by assuming a combination of Mohr–Coulomb and viscous behaviour without explicit elastic behaviour at low strains as we are interested in behaviour at higher strain. Details on parameter values used in the 3-layer model are provided in Table 1.

Failure is critically dependent on the initial cohesion of the competent layer (Fig. 2a;  $c_i$ ). It is also necessary to define the cohesion of the layer after failure and softening ( $c_s$ ). Here we define a cohesion ratio ( $R_{Co}$ ):

$$R_{Co} = c_i / c_s. \quad (5)$$

**Pinch and swell structures**

R. Gardner et al.

Title Page	
Abstract	Introduction
Conclusions	References
Tables	Figures
◀	▶
◀	▶
Back	Close
Full Screen / Esc	
Printer-friendly Version	
Interactive Discussion	



Both  $c_i$  and  $c_s$  values have no dimensions so provide relative rather than absolute information (Fig. 2a). This ratio is kept constant in the models except where the impact of  $c_s$  is specifically tested in analysis IV.

## 4.2 Model analysis

5 Numerical results were extracted from the model at regular intervals throughout the simulations. The results are plotted as spatial distributions of different particle properties, for example, layer affinity, strain rate, stress and viscosity. Results are extracted at different stretch values and are used to represent the model evolution. In addition, model results were analysed using canny edge detection methods in the Image Processing Toolbox<sup>TM</sup> in Matlab<sup>®</sup> to determine swell and neck widths and tortuosity. Tortuosity is the ratio of the competent edge length to the straight line length. A tortuosity of  $> 1.1$  was taken to indicate probable formation of pinch and swell structures. An additional ratio of the minimum neck width ( $W_N$ ) to the maximum swell width ( $W_S$ ) was measured using:

$$15 \quad R_W = W_N/W_S. \quad (6)$$

An  $R_W$  value  $< 0.4$  was taken to indicate successful pinch and swell initiation, a value  $< 0.2$  indicates successful formation of the pinch and swell structures and a value  $< 0.05$  indicates attenuation of the neck. In addition, to monitor the behaviour of the system at a local scale, “tracer” particles on a  $9 \times 5$  grid across the model were marked and their evolution followed throughout each numerical simulation. Differential stress, strain rate invariant, viscosity and pressure were collected on each step and have been used to produce the graphs presented.

## Pinch and swell structures

R. Gardner et al.

Title Page

Abstract

Introduction

Conclusions

References

Tables

Figures



Back

Close

Full Screen / Esc

Printer-friendly Version

Interactive Discussion



### 4.3 Three layer model

In order to evaluate the model behaviour and investigate the impact of flow property variations on pinch and swell structure characteristics, we systematically test their development:

5 *Analysis I: Effect of mode II failure and stress exponent:* To test if pinch and swell structures could be initiated by mode II failure and could form irrespective of the stress exponent, simulations were completed where layer B (Fig. 2b) had brittle Mohr–Coulomb behaviour, and all layers had either Newtonian flow ( $n = 1$ ) or non-Newtonian flow ( $n = 3$ ).  $R_V$  was set at 20 for this analysis. Other parameters in the models were  
10 as specified in Table 1.  $R_W$  was used to indicate successful pinch and swell initiation and formation.

*Analysis II: Impact of relative initial viscosity:* To test the impact of the competent layer to matrix initial viscosity ratio ( $R_V$ ) on the formation of pinch and swell structures we undertook additional simulations in non-Newtonian flow.  $R_V$  was increased until  
15 pinch and swell structures were successfully formed. Again,  $R_W$  was used to indicate successful pinch and swell initiation and formation.

*Analysis III: Impact of layer dependent flow properties:* To test the impact of brittle behaviour and flow regime across the layers in the model, four separate series of simulations with  $R_V$  set at 10 were undertaken (Table 2). We systematically varied the  
20 stress exponent and brittle behaviour: (1) all layers were given Newtonian flow, (2) matrix layers (A) were given Newtonian flow while layer B was given non-Newtonian flow ( $n = 3$ ), (3) layer B was given Newtonian flow while the matrix layers (A) were given non-Newtonian flow ( $n = 3$ ), (4) all layers were given non-Newtonian flow ( $n = 3$ ). Mohr–Coulomb behaviour was varied within each of these series (Table 1): (i) all layers  
25 were given Mohr–Coulomb behaviour; (ii) matrix layers (A) were given Mohr–Coulomb behaviour; (iii) only layer B had Mohr–Coulomb behaviour, (iv) no layers were given Mohr–Coulomb behaviour.

## SED

7, 1517–1554, 2015

### Pinch and swell structures

R. Gardner et al.

Title Page

Abstract

Introduction

Conclusions

References

Tables

Figures



Back

Close

Full Screen / Esc

Printer-friendly Version

Interactive Discussion



## Pinch and swell structures

R. Gardner et al.

Title Page

Abstract

Introduction

Conclusions

References

Tables

Figures

◀

▶

◀

▶

Back

Close

Full Screen / Esc

Printer-friendly Version

Interactive Discussion



*Analysis IV: impact of cohesion and material softening:* To test the impact of softening on the formation of pinch and swell structures a series of models with Newtonian flow ( $n = 1$ ), an  $R_V$  of 20 and Mohr–Coulomb behaviour in only layer B was used. Initial cohesion was not varied from the previous analyses and only the Underworld cohesion after softening ( $c_s$ ) parameter was varied giving  $R_{Co}$  values which ranged from 100, where there is a high degree of softening on those particles that yielded through 20, 10, 4, and 2, to 1 where there is no softening.

### 4.4 Multi-layer model

To explore the impact of brittle behaviour in the middle to lower crust on the pattern of strain localisation and near-surface structural development, a multi-layer model was developed to represent a crustal scale extensional scenario. In this model, a compressible layer at the top (Fig. 2d layer D) allows topography to develop (Hetényi et al., 2011) and a brittle layer (Fig. 2d layer C, with Mohr–Coulomb behaviour) represents the upper continental crust reaching the surface. Five layers (Fig. 2d, A' and B' layers) of alternating material properties, similar to our 3-layer model, represent the middle to lower continental crust. The relative widths and viscosity ratio ( $R_V = 20$ ) of these A' and B' layers are the same as for the three layer model. We present results from two simulations where the rheological properties of the lower 5 layers (i.e. A' and B' layers) are varied. The model was run with non-Newtonian ( $n = 3$ ) flow. In model (a) layers A' and B' have purely viscous rheological properties with no brittle Mohr–Coulomb behaviour, while in model (b) the B' layers were given Mohr–Coulomb brittle behaviour.

## 5 Results

### 5.1 General model behaviour

Flow property testing of the Underworld stress exponent and yielding parameters on a single material  $1 \times 1$  model ensured flow behaviour according to theoretical predic-

tions (Fig. S1). Model results (Fig. 3a) show the development of the pinch and swell structures and the movement of the planar features. The neck and swell development can be seen most clearly in the strain rate invariant results (Fig. 3b). The inverse relationship between strain rate and stress (per Eq. 1) can be seen in Fig. 3b and c. Where strain rate is high (Fig. 3b dark bands), the equivalent area in the stress results has low stress values (Fig. 3c light areas) and the planar features in the material results (Fig. 3a) become distorted. The viscosity, strain rate and differential stress values were plotted (Fig. 3d–f) for selected particles within the competent layer (Fig. 3a–c red, green and black star locations). The black particle has relatively higher strain rate and lower stress as it is in an area that subsequently develops into a neck. By contrast, the red and green particles are in relatively low strain, higher stress areas that develop into swells. As the example shown has a stress exponent of three ( $n = 3$ ), there is also an inverse relationship between viscosity and strain rate (Fig. 3d and e). These graphs show the model is working as theoretically expected for a yielding material (compare Fig. 3f with Fig. 2c).

## 5.2 Analysis I: effect of mode II failure and stress exponent

The progressive development of the pinch and swell structure is shown in Fig. 4 at  $R_V = 20$  for both Newtonian (Fig. 4a; Fig. 5a dashed black line) and non-Newtonian (Fig. 4b; Fig. 5a solid black line) flow. Where the competent layer had no brittle behaviour (Fig. 5a black dotted line), no change in the layer width was seen as the model stretched and thinned, so  $R_W$  remained at 1. The positions for the formation of the necks are defined by the mode II brittle failure surfaces initiated at low stretch values, early in the simulations. These failure surfaces, where the strain localises to form local shear bands at  $\sim 40^\circ$  to the stretching direction, can be seen in the strain rate invariant results at each stretch value (Fig. 4). As the stretch increases (Fig. 4), the layers are elongated and thinned. The necks thin more quickly than the swells causing the marker beds to distort near the localisation of strain in the neck (Figs. 3a and 4) and the pinch

### Pinch and swell structures

R. Gardner et al.

Title Page

Abstract

Introduction

Conclusions

References

Tables

Figures



Back

Close

Full Screen / Esc

Printer-friendly Version

Interactive Discussion



and swell structures to be more obvious at higher stretch values (Figs. 4a and 5a black lines,  $n = 1$  dashed,  $n = 3$  solid).

Some swell structures display rotation of the passive marker beds as the strain localisation is established (Figs. 4 and 5b to stretch 1.6). Where the strain localisation is regularly distributed ( $\pm \sim 40^\circ$  to vertical) this results in swells with the passive beds rotating up to  $\pm 5^\circ$  (Fig. 4b). At higher stretch values these become curved parallel to the edge of the swell to matrix interface. Where the strain localisation is not regularly distributed, that is, one direction dominates (e.g. Fig. 5b swell 1 and 2), this results in swells with the passive beds rotating up to  $\pm 15^\circ$ .

Figure 4 shows the localisation of strain to just a few failure planes is more effective in Newtonian (Fig. 4a) than non-Newtonian (Figs. 4b and 5a) flow regimes in this model. The increased number of brittle failure planes for our non-Newtonian flow model results in weaker isolation of the swell structures. At the same strain, the pinch and swell structures are more separated and defined in Newtonian flow than in non-Newtonian flow (for example, Fig. 4 stretch 1.6; Fig. 5a black dashed and solid lines).

### 5.3 Analysis II: effect of relative initial viscosity ratio ( $R_V$ )

The viscosity of the matrix layers (A) was varied to see the impact of  $R_V$  on the formation of pinch and swell structures (Fig. 5a). The ratio of the neck width to swell width ( $R_W$ ) for the series (Fig. 5a) shows that  $R_W$  decreases as  $R_V$  increases, indicating better formation of pinch and swell structures at higher  $R_V$  values. For Newtonian flow, pinch and swell structures were successfully initiated (i.e.  $R_W < 0.4$ ) from  $R_V = 10$ , while for non-Newtonian flow this was not the case until  $R_V = 125$  (Fig. 5a).

### 5.4 Analysis III: effect of layer dependent flow property behaviour

A summary of results where the Newtonian and non-Newtonian flow and Mohr–Coulomb behaviour of the matrix layers (A) vs. competent layer (B layer) was systematically varied is provided in Table 2. Fig. S2 shows numerical results at stretch 2.3.

## Pinch and swell structures

R. Gardner et al.

Title Page

Abstract

Introduction

Conclusions

References

Tables

Figures



Back

Close

Full Screen / Esc

Printer-friendly Version

Interactive Discussion



Pinch and swell structures form where layer B has Mohr–Coulomb brittle behaviour (Table 2, rows i and iii) and do not form where layer B does not have Mohr–Coulomb behaviour (Table 2 rows ii and iv). The results show that the Mohr–Coulomb behaviour of the matrix layers (A) does not impact the formation of pinch and swell structures.

5 The results also show pinch and swell structures can form in both Newtonian and non-Newtonian flow in all flow regime combinations of matrix vs. competent layer (Table 2, rows i and iii) where at least layer B has Mohr–Coulomb behaviour.

### 5.5 Analysis IV: effect of cohesion and material softening

10 Good pinch and swell development is shown for all models where  $R_{Co} > 1$  (Fig. 6a–e and h;  $R_W < 0.2$ ). The average tortuosity of the two competent layer edges in each model (plotted in Fig. 6h) shows a gradual increase as  $R_{Co}$  increases to  $R_{Co} = 10$  where it plateaus. This corresponds to an increasing complexity of pinch and swell structures where  $R_{Co} > 10$  (Figs. 6a–c). Stretch to differential stress graphs of the different cohesion ratios (Fig. 6g) show a sharp drop in stress after the material has failed.

15 Where the material is softer after fracturing (higher  $R_{Co}$  values) the stress is lower, though high levels of softening ( $R_{Co} = 20$  and 100) show similar differential stress levels. The softened material shows some variability immediately after yielding (as suggested by Griggs and Handin, 1960), but then stabilizes to constant stress at larger stretch values. High levels of material softening ( $R_{Co} = 100$ ) also appear to impact strain localisation, as an area of thick neck that has not formed a pinch and swell structure can be seen (Fig. 6a, black arrow).

### 5.6 Multi-layer model: impact of brittle behaviour on surface topology

Model results at stretch 2.3 show the development of near surface structure, layer shape and the distribution of strain rate throughout the crustal scale model (Fig. 7).

25 Where the lowest five layers, i.e. the middle to lower crust have non-brittle behaviour (Fig. 7a; A' and B' layers), strain is localised only in the upper layer, leading to fewer

## Pinch and swell structures

R. Gardner et al.

Title Page

Abstract

Introduction

Conclusions

References

Tables

Figures



Back

Close

Full Screen / Esc

Printer-friendly Version

Interactive Discussion





areas of focused localisation. This causes very simple near surface faulting and a relatively low  $R_W$  value allowing the lower layers to be closer to the surface. Where some of the middle to lower crustal layers (i.e. B' layers), were given Mohr–Coulomb brittle behaviour (Fig. 7b) representing a heterogeneous rheological behaviour, strain localisation is strongest in the upper crust (blue layer), but occurs across all layers leading to relatively dispersed strain localisation. This causes increased complexity of the near-surface faulting and a relatively higher  $R_W$  value with the lower layers further from the surface. Significant rotation of the planar beds to  $\pm 23^\circ$  is seen in both models though this is more prominent in model (a) as the strain is localised predominantly in a single direction. Surface tortuosity (Fig. 7c dashed lines) is very similar between the models up to stretch  $\sim 2$ . As the stretch increases above 2, surface tortuosity decreases more slowly in model (b) than in model (a) (Fig. 7b).

## 6 Discussion

### 6.1 Pinch and swell initiation by brittle deformation

Our model successfully initiates pinch and swell structures using mode II Mohr–Coulomb brittle failure and allows the structures to develop in subsequent viscous flow. This indicates that combining brittle and viscous behaviour is a plausible rheological model for producing pinch and swell structures. The main difference between our model and the model used by Abe and Urai (2012) and Komoróczy et al. (2013) is the type of brittle structures initiating pinch and swell structures; namely mode II vs. mode I brittle deformation.

Our results support Mancktelow (2006) who concluded that ductile shear zones form after Mohr–Coulomb brittle failure at middle to lower continental crust depths. Mancktelow (2006) suggests that ductile flow with fluid influx requires ongoing pressure dependent brittle failures, including micro-cracking for fluid to continue to flow into the shear zone. The thin section scale brittle failures observed in the St. Anne Point

## Pinch and swell structures

R. Gardner et al.

Title Page

Abstract

Introduction

Conclusions

References

Tables

Figures



Back

Close

Full Screen / Esc

Printer-friendly Version

Interactive Discussion



## Pinch and swell structures

R. Gardner et al.

Title Page

Abstract

Introduction

Conclusions

References

Tables

Figures



Back

Close

Full Screen / Esc

Printer-friendly Version

Interactive Discussion



samples (Fig. 1d and e) are likely examples of the micro-cracking he invokes. This micro-cracking develops into through-going micro-shear bands (Fig. 1e, dashed line) which are then inferred to develop into outcrop scale shear bands. In material science, a shear band forms where strain induced softening factors (thermal and/or geometric) dominate the strain and strain-rate hardening factors (Meyers, 1994). Where this formation of shear bands by plastic deformation is followed by slow crack propagation it is called a “ductile fracture”, compared with a brittle fracture which has little plastic deformation and fast crack propagation (Meyers, 1994). Our numerical simulations reproduce these “ductile fractures” suggesting that pinch and swell structures can be formed through “ductile fracturing”.

### 6.2 Effect of stress exponent, brittle behavior, $R_V$ and $R_{Co}$ for the competent layer and matrix

Analysis III shows that brittle failure of at least the competent layer is required for pinch and swell structures to form. Analysis I and II show that pinch and swell structures form readily in Newtonian flow (Fig. 4a) from viscosity ratios of  $\sim 10$ , but in non-Newtonian flow (Figs. 4b and 5) they form only at much larger viscosity ratios of  $\sim 125$ . This result contrasts with other researchers who suggest pinch and swell structures can only form where the stress exponent ( $n$ )  $> 1$  (Schmalholz and Maeder, 2012; Smith, 1977). It should be noted that our results are not directly comparable to these studies as their layers are purely viscous and the competent layer required an initial irregularity, or instability to grow to initiate the pinch and swell structure. By contrast, we use brittle deformation for pinch and swell structure initiation and viscous flow for only post failure structure development. Nor are our results directly comparable to the experiments by (Abe and Urai, 2012; Komoróczy et al., 2013) as they have used mode I brittle fracture to initiate the structures while we have modelled mode II fracturing.

Komoróczy et al. (2013) who used mode I brittle fracture for pinch and swell structure initiation indicated that the matrix viscosity impacts the number of swell structures

formed. Our model suggests this is possibly due to the impact of the viscosity ratio on the localisation of strain to form the brittle failures that initiate the structure formation.

Many authors have previously suggested material softening is required for pinch and swell formation (Hobbs et al., 2009; Neurath and Smith, 1982, 1977; van der Molen, 1985). Our results from analysis IV is in general agreement with the latter conclusions, as the degree of softening after failure has a marked effect on the nature of the developing pinch and swell structure (Fig. 6). At low levels of softening (low  $R_{Co}$ ) simple symmetric pinch and swell structures are formed while at higher levels more complex structures develop (Fig. 6). These differences in behaviour, can be utilized in the interpretation of pinch and swell structures. For example, the presence of thick necks in the pinch and swell chain indicates strong softening within a failure zone relative to its original strength.

In nature, material softening is caused by numerous processes such as grain size reduction and metamorphic reactions resulting in different assemblages. Grain size reduction may occur either by deformation (e.g. Bestmann and Prior, 2003; Fliervoet et al., 1997; Herwegh et al., 2011; Krabbendam et al., 2003; Kruse and Stünitz, 1999) or reaction (e.g. Brodie and Rutter, 1985, 1987; Piazzolo and Jaconelli, 2014; Rubie, 1990, 1983; Smith et al., 2015). Assemblage variation due to partial or complete metamorphic reaction with “softer” phases have been reported to induce strain localization (Brodie and Rutter, 1985, 1987; de Ronde et al., 2005; Holyoke III and Tullis, 2006; Newman et al., 1999; Rubie, 1990, 1983; Stünitz and Tullis, 2001; Watts and Williams, 1983). Material softening may occur to variable degrees even if the same process of softening is involved. For example, grain size reduction can cause limited softening when the new grain size is still dominantly in grain size insensitive, power law flow, however, a transition to grain size sensitive Newtonian flow regime through grain size reduction can cause significant levels of softening (e.g. Smith et al., 2015). Our numerical scheme using a rheological model combining Mohr–Coloumb and viscous flow allows simulation of this wide range of softening behaviours observed in nature by varying  $R_{Co}$ .

## SED

7, 1517–1554, 2015

### Pinch and swell structures

R. Gardner et al.

Title Page

Abstract

Introduction

Conclusions

References

Tables

Figures



Back

Close

Full Screen / Esc

Printer-friendly Version

Interactive Discussion



### 6.3 Application of the numerical model to field interpretation

Analysis I (Fig. 4) allows three stages of pinch and swell structure to be distinguished (Fig. 5a) as the structures develop with decreasing  $R_W$  and increasing stretch:

Stage 1, where zones of localised strain are establishing and the structures have not started to form:  $0.4 < R_W < 0.75$  (e.g. Fig. 4a stretch 1.2 to 1.6; Fig. 5a).

Stage 2, where the strain has localised and pinch and swell structures have successfully been initiated and are starting to separate:  $0.2 < R_W < 0.4$  (e.g. Fig. 4a stretch 1.6 to 2.5; Fig. 5a).

Stage 3, where the pinch and swell structures have successfully formed and are well defined and separated:  $R_W < 0.2$  (e.g. Fig. 4a stretch 2.5 to 3.2; Fig. 5a). Attenuation of the neck is developed where  $R_W < 0.05$ .

The numerical model can also provide some additional insights into the processes forming the pinch and swell structures: (i) rotation  $> 5^\circ$  of once planar structures in the swell structures indicates uneven strain localisation on the brittle deformation conjugate sets, (ii) tortuosity of the competent layer edges  $> 1.2$  and/or complex pinch and swell formations suggest significant material softening after brittle deformation of the competent layer, (iii) the presence of a thick neck suggests very strong material softening after the initial brittle deformation, (iv) the ratio of neck width to swell width can be compared with the three stages of pinch and swell structure development (Fig. 5a) and a general idea of the relative layer viscosities can be deduced. However, for a more accurate determination, both Newtonian vs. non-Newtonian flow and stretch should be independently validated by complementary methods (e.g. strain markers and microstructures).

In the following, we show the applicability of our model result to nature by comparison with the field data from the pinch and swell structures observed on the St. Anne Point rock platform. Our model suggests brittle failure of at least the competent layer is required for the St. Anne Point pinch and swell structures to form. The natural pinch and swell structures show both stage 2 development with  $R_W < 0.4$  (Fig. 1c) and stage 3 development, with  $R_W < 0.2$  (Fig. 1a and b). Rotation of the bedding greater than  $5^\circ$

SED

7, 1517–1554, 2015

## Pinch and swell structures

R. Gardner et al.

Title Page

Abstract

Introduction

Conclusions

References

Tables

Figures

◀

▶

◀

▶

Back

Close

Full Screen / Esc

Printer-friendly Version

Interactive Discussion



can be seen in Fig. 1c, similar to that seen in the models where fracturing was dominated by one direction (Figs. 4a and 5b). This and the presence of both stage 2 and 3 development suggest strain localisation was spread unevenly across the rock platform.

Thin section analysis showed the St. Anne Point samples display non-Newtonian flow. Therefore, comparison of model results (Fig. 5a) and nature (Fig. 1a and b) predicts a high viscosity ratio ( $R_V > 125$ ) between the mafic pinch and swell layer and the surrounding paragneiss. At the same time, the St. Anne Point pinch and swell chain (Fig. 1a and b) has good separation of swell structures with attenuated necks (Fig. 1a and b black arrows) and shows locally, a thick neck (Fig. 1b black arrow). Accordingly, a high degree of softening i.e. larger  $R_{Co}$  value (Fig. 6a, black arrow) is expected for these rocks.

#### 6.4 Implications of the presence of brittle-viscous behaviour in the middle to lower continental crust

Pinch and swell structures are commonly observed from amphibolite facies terranes (e.g. Goscombe et al., 2004; Hobbs et al., 2010; van der Molen, 1985), supporting the interpretation that middle to lower crustal rocks are heterogeneous in terms of both viscous flow properties and brittle vs. ductile behaviour. This is consistent with the growing evidence that the flow behaviour of middle to lower continental crust should not be considered as exclusively viscous (e.g. Mancktelow, 2006).

Our crustal scale numerical model (Fig. 7) suggests large scale structures associated with strain localization penetrating from the upper crust into the middle and lower crust can be explained by the presence of some rock units exhibiting brittle deformation in the middle and lower crust. If the middle to lower continental crust deforms by only viscous deformation (i.e. layers A' and B', Fig. 2d, are exclusively viscous), all layers except the brittle surface crust (layer C), are ductile and there is no significant localisation of the strain into the lower crust (Fig. 7a) unless extremely high stress exponent ( $n$ ) values are inferred for non-Newtonian flow. However, including a subset of brittle layers (B' layers in Fig. 2d) in the middle to lower crust model (Fig. 7b) causes strain

### Pinch and swell structures

R. Gardner et al.

Title Page

Abstract

Introduction

Conclusions

References

Tables

Figures



Back

Close

Full Screen / Esc

Printer-friendly Version

Interactive Discussion



**Pinch and swell structures**

R. Gardner et al.

Title Page

Abstract

Introduction

Conclusions

References

Tables

Figures

I◀

▶I

◀

▶

Back

Close

Full Screen / Esc

Printer-friendly Version

Interactive Discussion



localisation zones to extend from the surface layer (Fig. 7 layer C) into the mid and lower crustal sections i.e. A' and B' layers. This continuous strain localization within the whole crustal section can, for example, explain geophysical data (e.g. Middleton et al., 1993) suggesting strain localization may indeed be continuous from upper to lower crustal levels. At the same time, such a pattern of strain localization will have considerable impact on the pattern of near-surface structures (Fig. 7b). In summary, the pattern of strain localization is highly influenced by the presence or absence of brittle-viscous layers. Hence, surface features, fluid influx pathways and, therefore, ore genesis, are highly dependent on the heterogeneous nature of the middle and lower crust in terms of brittle-viscous vs. viscous behaviour.

The fact that pinch and swell structures are commonly observed at all crustal levels (Arslan et al., 2008; Goscombe et al., 2004; Hobbs et al., 2010; Kenis et al., 2004; Ponce et al., 2013; van der Molen, 1985) suggests that it is necessary to include brittle-viscous behaviour in both small- and crustal-scale models of deformation within the Earth's crust.

## 7 Conclusion

Our numerical model, using brittle, mode II deformation to initiate pinch and swell structures followed by viscous flow indicates: (i) these structures can form in either Newtonian or non-Newtonian flow contrary to previous conclusions where only viscous flow was used, (ii) higher viscosity ratios are required for pinch and swell formation in non-Newtonian regimes, (iii) material softening in the competent layer is needed for their development; and (iv) the matrix stress exponent and brittle behaviour have little influence on pinch and swell formation itself.

We suggest that measuring planar bedding rotation, neck to swell thickness ratio ( $R_W$ ) and tortuosity on a pinch and swell structure can provide important insights into the localisation of strain and flow properties (e.g. stress exponent, relative viscosity and degree of softening) of both the competent and matrix layers.

## Pinch and swell structures

R. Gardner et al.

Title Page

Abstract

Introduction

Conclusions

References

Tables

Figures



Back

Close

Full Screen / Esc

Printer-friendly Version

Interactive Discussion



Incorporation of brittle-viscous behaviour in some rock units at middle to lower crustal levels (i) has a significant impact on the pattern of strain localisation throughout the continental crust and the development of near surface structures and (ii) can explain the development of crustal scale structures observed in nature. Consequently, we suggest that the inclusion of Mohr Coulomb brittle fracturing and viscous flow is necessary when developing crustal scale numerical models.

**The Supplement related to this article is available online at doi:10.5194/sed-7-1517-2015-supplement.**

*Acknowledgements.* Logistical and analytical funding was provided by an MQRes scholarship (RG), Discovery Project (DP120102060 to SP and NRD), Future Fellowship (FT1101100070 to SP) and internal funding from the Department of Earth and Planetary Sciences, Macquarie University. Code development in Underworld was supported by the Victorian Partnership for Advanced Computing and Monash University (Moresi et al., 2003, 2007). We thank the Department of Conservation in Te Anau for permission to visit and sample localities within St. Anne Point, Fiordland National Park and David Keith of the School of Environment and Rural Science, University of New England for thin section preparation. The authors would also like to thank two anonymous reviewers for their careful and constructive reviews, and N. Mancktelow for editorial handling.

## References

- Abe, S. and Urai, J. L.: Discrete element modeling of boudinage: insights on rock rheology, matrix flow, and evolution of geometry, *J. Geophys. Res.-Sol. Ea.*, 117, B01407, doi:10.1029/2011jb008555, 2012.
- Arslan, A., Passchier, C. W., and Koehn, D.: Foliation boudinage, *J. Struct. Geol.*, 30, 291–309, doi:10.1016/j.jsg.2007.11.004, 2008.
- Bestmann, M. and Prior, D. J.: Intragranular dynamic recrystallization in naturally deformed calcite marble: diffusion accommodated grain boundary sliding as a result of subgrain rota-

**Pinch and swell structures**

R. Gardner et al.

Title Page

Abstract

Introduction

Conclusions

References

Tables

Figures

I◀

▶I

◀

▶

Back

Close

Full Screen / Esc

Printer-friendly Version

Interactive Discussion



tion recrystallization, *J. Struct. Geol.*, 25, 1597–1613, doi:10.1016/S0191-8141(03)00006-3, 2003.

Brander, L., Svahnberg, H., and Piazzolo, S.: Brittle-plastic deformation in initially dry rocks at fluid-present conditions: transient behaviour of feldspar at mid-crustal levels, *Contrib. Mineral. Petr.*, 163, 403–425, doi:10.1007/s00410-011-0677-5, 2012.

Brodie, K. H. and Rutter, E. H.: On the Relationship between Deformation and Metamorphism, with Special Reference to the Behavior of Basic Rocks, in: *Metamorphic Reactions, Advances in Physical Geochemistry*, edited by: Thompson, A. and Rubie, D., Springer-Verlag, Berlin, Heidelberg, New York, Tokyo, 138–179, 1985.

Brodie, K. H. and Rutter, E. H.: Deep crustal extensional faulting in the Ivrea Zone of Northern Italy, *Tectonophysics*, 140, 193–212, doi:10.1016/0040-1951(87)90229-0, 1987.

de Ronde, A. A., Stünitz, H., Tullis, J., and Heilbronner, R.: Reaction-induced weakening of plagioclase-olivine composites, *Tectonophysics*, 409, 85–106, doi:10.1016/j.tecto.2005.08.008, 2005.

Emerman, S. H. and Turcotte, D. L.: A back-of-the-envelope approach to boudinage mechanics, *Tectonophysics*, 110, 333–338, doi:10.1016/0040-1951(84)90267-1, 1984.

Fliervoet, T. F., White, S. H., and Drury, M. R.: Evidence for dominant grain-boundary sliding deformation in greenschist- and amphibolite-grade polymineralic ultramylonites from the Redbank Deformed Zone, Central Australia, *J. Struct. Geol.*, 19, 1495–1520, doi:10.1016/S0191-8141(97)00076-X, 1997.

Fusseis, F., Handy, M. R., and Schrank, C.: Networking of shear zones at the brittle-to-viscous transition (Cap de Creus, NE Spain), *J. Struct. Geol.*, 28, 1228–1243, doi:10.1016/j.jsg.2006.03.022, 2006.

Goldstein, A. G.: Factors affecting the kinematic interpretation of asymmetric boudinage in shear zones, *J. Struct. Geol.*, 10, 707–715, doi:10.1016/0191-8141(88)90078-8, 1988.

Goscombe, B. D., Passchier, C. W., and Hand, M.: Boudinage classification: end-member boudin types and modified boudin structures, *J. Struct. Geol.*, 26, 739–763, doi:10.1016/j.jsg.2003.08.015, 2004.

Griggs, D. and Handin, J.: Observations on fracture and a hypothesis of earthquakes, *Geol. Soc. Am. Mem.*, 79, 347–364, 1960.

Guermani, A. and Pennacchioni, G.: Brittle precursors of plastic deformation in a granite: an example from the Mont Blanc massif (Helvetic, western Alps), *J. Struct. Geol.*, 20, 135–148, doi:10.1016/S0191-8141(97)00080-1, 1998.



**Pinch and swell structures**

R. Gardner et al.

Title Page

Abstract

Introduction

Conclusions

References

Tables

Figures

◀

▶

◀

▶

Back

Close

Full Screen / Esc

Printer-friendly Version

Interactive Discussion



- Herwegh, M., Linckens, J., Ebert, A., Berger, A., and Brodhag, S. H.: The role of second phases for controlling microstructural evolution in polymineralic rocks: a review, *J. Struct. Geol.*, 33, 1728–1750, doi:10.1016/j.jsg.2011.08.011, 2011.
- 5 Hetényi, G., Godard, V., Cattin, R., and Connolly, J. A. D.: Incorporating metamorphism in geodynamic models: the mass conservation problem, *Geophys. J. Int.*, 186, 6–10, doi:10.1111/j.1365-246X.2011.05052.x, 2011.
- Hirth, G. and Kohlstedt, D.: Rheology of the Upper Mantle and the mantle wedge: a view from the experimentalists, in: *Inside the Subduction Factory*, American Geophysical Union, 83–105, 2003.
- 10 Hobbs, B. E., Regenauer-Lieb, K., and Ord, A.: Folding with thermal-mechanical feedback: a reply, *J. Struct. Geol.*, 31, 752–755, doi:10.1016/j.jsg.2009.03.014, 2009.
- Hobbs, B. E., Ord, A., Spalla, M. I., Gosso, G., and Zucali, M.: The interaction of deformation and metamorphic reactions, *London, Geol. Soc. Spec. Publ.*, 332, 189–223, doi:10.1144/sp332.12, 2010.
- 15 Holyoke Iii, C. W. and Tullis, J.: Mechanisms of weak phase interconnection and the effects of phase strength contrast on fabric development, *J. Struct. Geol.*, 28, 621–640, doi:10.1016/j.jsg.2006.01.008, 2006.
- Kenis, I., Urai, J. L., van der Zee, W., and Sintubin, M.: Mullions in the High-Ardenne Slate Belt (Belgium): numerical model and parameter sensitivity analysis, *J. Struct. Geol.*, 26, 1677–1692, doi:10.1016/j.jsg.2004.02.001, 2004.
- 20 Klepeis, K. A., Daczko, N. R., and Clarke, G. L.: Kinematic vorticity and tectonic significance of superposed mylonites in a major lower crustal shear zone, northern Fiordland, New Zealand, *J. Struct. Geol.*, 21, 1385–1405, doi:10.1016/S0191-8141(99)00091-7, 1999.
- Kobberger, G. and Zulauf, G.: Experimental folding and boudinage under pure constrictional conditions, *J. Struct. Geol.*, 17, 1055–1063, doi:10.1016/0191-8141(94)00130-R, 1995.
- 25 Koehn, D., Arnold, J., and Passchier, C. W.: Fracture and vein patterns as indicators of deformation history: a numerical study, *Geological Society, London, Special Publications*, 243, 11–24, 2005.
- Komoróczy, A., Abe, S., and Urai, J.: Meshless numerical modeling of brittle-viscous deformation: first results on boudinage and hydrofracturing using a coupling of discrete element method (DEM) and smoothed particle hydrodynamics (SPH), *Comput. Geosci*, 17, 373–390, doi:10.1007/s10596-012-9335-x, 2013.
- 30

**Pinch and swell structures**

R. Gardner et al.

Title Page

Abstract

Introduction

Conclusions

References

Tables

Figures

I◀

▶I

◀

▶

Back

Close

Full Screen / Esc

Printer-friendly Version

Interactive Discussion



- Krabbendam, M., Urai, J. L., and van Vliet, L. J.: Grain size stabilisation by dispersed graphite in a high-grade quartz mylonite: an example from Naxos (Greece), *J. Struct. Geol.*, 25, 855–866, doi:10.1016/S0191-8141(02)00086-X, 2003.
- 5 Kruse, R. and Stünitz, H.: Deformation mechanisms and phase distribution in mafic high-temperature mylonites from the Jotun Nappe, southern Norway, *Tectonophysics*, 303, 223–249, doi:10.1016/S0040-1951(98)00255-8, 1999.
- Lohest, M., Stainier, X., and Fourmarier, P.: Compte rendu de la session extraordinaire de la Société géologique de Belgique, tenue à Eupen et Bastogne les 29, 30 et 31 août et le 1, 2 et 3 Septembre 1908, *Annales de la Société géologique de Belgique*, 36, 275–282, 1908.
- 10 Mancktelow, N. S.: How ductile are ductile shear zones?, *Geology*, 34, 345–348, doi:10.1130/g22260.1, 2006.
- Mancktelow, N. S. and Pennacchioni, G.: The control of precursor brittle fracture and fluid–rock interaction on the development of single and paired ductile shear zones, *J. Struct. Geol.*, 27, 645–661, doi:10.1016/j.jsg.2004.12.001, 2005.
- 15 Marques, F. O., Fonseca, P. D., Lechmann, S., Burg, J.-P., Marques, A. J. M., and Alves, C.: Boudinage in nature and experiment, *Tectonophysics*, 526–529, 88–96, doi:10.1016/j.tecto.2011.08.017, 2012.
- Mengong, M. E. and Zulauf, G.: Coeval folding and boudinage under plane strain with the axis of no change perpendicular to the layer, *Int. J. Earth Sci.*, 95, 178–188, doi:10.1007/s00531-005-0032-z, 2006.
- Meyers, M. A.: *Dynamic Behavior of Materials*, Wiley, New York, 668 pp., 1994.
- Middleton, M., Wilde, S., Evans, B., Long, A., and Dentith, M.: A preliminary interpretation of deep seismic reflection and other geophysical data from the Darling Fault Zone, Western Australia, *Explor. Geophys.*, 24, 711–718, 1993.
- 25 Molnar, P. and Houseman, G. A.: The effects of buoyant crust on the gravitational instability of thickened mantle lithosphere at zones of intracontinental convergence, *Geophys. J. Int.*, 158, 1134–1150, doi:10.1111/j.1365-246X.2004.02312.x, 2004.
- Moresi, L. and Mühlhaus, H. B.: Anisotropic viscous models of large-deformation Mohr–Coulomb failure, *Philos. Mag.*, 86, 3287–3305, doi:10.1080/14786430500255419, 2006.
- 30 Moresi, L., Dufour, F., and Mühlhaus, H. B.: A Lagrangian integration point finite element method for large deformation modeling of viscoelastic geomaterials, *J. Comput. Phys.*, 184, 476–497, doi:10.1016/S0021-9991(02)00031-1, 2003.

**Pinch and swell structures**

R. Gardner et al.

Title Page

Abstract

Introduction

Conclusions

References

Tables

Figures

I◀

▶I

◀

▶

Back

Close

Full Screen / Esc

Printer-friendly Version

Interactive Discussion



- Moresi, L., Quenette, S., Lemiale, V., Mériaux, C., Appelbe, B., and Mühlhaus, H. B.: Computational approaches to studying non-linear dynamics of the crust and mantle, *Phys. Earth Planet. In.*, 163, 69–82, doi:10.1016/j.pepi.2007.06.009, 2007.
- Neurath, C. and Smith, R. B.: The effect of material properties on growth rates of folding and boudinage: experiments with wax models, *J. Struct. Geol.*, 4, 215–229, doi:10.1016/0191-8141(82)90028-1, 1982.
- Newman, J., Lamb, W. M., Drury, M. R., and Vissers, R. L. M.: Deformation processes in a peridotite shear zone: reaction-softening by an H<sub>2</sub>O-deficient, continuous net transfer reaction, *Tectonophysics*, 303, 193–222, doi:10.1016/S0040-1951(98)00259-5, 1999.
- Passchier, C. W. and Trouw, R. A. J.: *Microtectonics*, Springer-Verlag, Berlin, 289 pp., 2005.
- Passchier, C. W., Mancktelow, N. S., and Grasemann, B.: Flow perturbations: a tool to study and characterize heterogeneous deformation, *J. Struct. Geol.*, 27, 1011–1026, doi:10.1016/j.jsg.2005.01.016, 2005.
- Piazolo, S. and Jaconelli, P.: Sillimanite deformation mechanisms within a Grt-Sil-Bt gneiss: effect of pre-deformation grain orientations and characteristics on mechanism, slip-system activation and rheology, *London, Geol. Soc. Spec. Publ.*, 394, 189–213, doi:10.1144/sp394.10, 2014.
- Pollard, D. and Segall, P.: Theoretical displacements and stresses near fractures in rock: with applications to faults, joints, veins, dikes, and solution surfaces, in: *Fracture Mechanics of Rock*, edited by: Atkinson, B., Academic Press, London, 277–349, 1987.
- Ponce, C., Druguet, E., and Carreras, J.: Development of shear zone-related lozenges in foliated rocks, *J. Struct. Geol.*, 50, 176–186, doi:10.1016/j.jsg.2012.04.001, 2013.
- Ramsay, A.: *The geology of North Wales*, *Memoirs of the Geological Survey of Great Britain*, London, UK, 3, 1866.
- Ramsay, J. G.: Shear zone geometry: a review, *J. Struct. Geol.*, 2, 83–99, doi:10.1016/0191-8141(80)90038-3, 1980.
- Ranalli, G.: *Rheology of the lithosphere in space and time*, *London, Geol. Soc. Spec. Publ.*, 121, 19–37, doi:10.1144/gsl.sp.1997.121.01.02, 1997.
- Rubie, D.: Role of kinetics in the formation and preservation of eclogites, in: *Eclogite Facies Rocks*, edited by: Carswell, D., Blackie, Glasgow, 111–140, 1990.
- Rubie, D. C.: Reaction-enhanced ductility: the role of solid-solid univariant reactions in deformation of the crust and mantle, *Tectonophysics*, 96, 331–352, doi:10.1016/0040-1951(83)90225-1, 1983.

**Pinch and swell structures**

R. Gardner et al.

Title Page

Abstract

Introduction

Conclusions

References

Tables

Figures



Back

Close

Full Screen / Esc

Printer-friendly Version

Interactive Discussion



- Rudnick, R. and Gao, S.: Composition of the continental crust, *Treatise on geochemistry*, 3, 1–64, 2003.
- Rybacki, E. and Dresen, G.: Deformation mechanism maps for feldspar rocks, *Tectonophysics*, 382, 173–187, 2004.
- 5 Schmalholz, S. M. and Maeder, X.: Pinch-and-swell structure and shear zones in viscoplastic layers, *J. Struct. Geol.*, 37, 75–88, doi:10.1016/j.jsg.2012.01.026, 2012.
- Scholz, C. H.: *The mechanics of earthquakes and faulting*, 2nd ed., Cambridge University Press, Cambridge, 473 pp., 2002.
- 10 Segall, P. and Simpson, C.: Nucleation of ductile shear zones on dilatant fractures, *Geology*, 14, 56–59, doi:10.1130/0091-7613(1986)14<56:nodszo>2.0.co;2, 1986.
- Simpson, C.: Deformation of granitic rocks across the brittle-ductile transition, *J. Struct. Geol.*, 7, 503–511, doi:10.1016/0191-8141(85)90023-9, 1985.
- 15 Smith, J., Piazzolo, S., Daczko, N., and Evans, L.: The effect of pre-tectonic reaction and annealing extent on behaviour during subsequent deformation: insights from paired shear zones in the lower crust of Fiordland, New Zealand, *J. Metamorph. Geol.*, doi:10.1111/jmg.12132, online first, 2015.
- Smith, R. B.: Unified theory of the onset of folding, boudinage, and mullion structure, *Geol. Soc. Am. Bull.*, 86, 1601–1609, doi:10.1130/0016-7606(1975)86<1601:utotoo>2.0.co;2, 1975.
- 20 Smith, R. B.: Formation of folds, boudinage, and mullions in non-Newtonian materials, *Geol. Soc. Am. Bull.*, 88, 312–320, doi:10.1130/0016-7606(1977)88<312:fofbam>2.0.co;2, 1977.
- St-Onge, M. R., Van Gool, J. A. M., Garde, A. A., and Scott, D. J.: Correlation of Archaean and Palaeoproterozoic units between northeastern Canada and western Greenland: constraining the pre-collisional upper plate accretionary history of the Trans-Hudson orogen, *London, Geol. Soc. Spec. Publ.*, 318, 193–235, doi:10.1144/sp318.7, 2009.
- 25 Stipp, M., Stünitz, H., Heilbronner, R., and Schmid, S. M.: The eastern Tonale fault zone: a “natural laboratory” for crystal plastic deformation of quartz over a temperature range from 250 to 700, *J. Struct. Geol.*, 24, 1861–1884, doi:10.1016/S0191-8141(02)00035-4, 2002.
- Stünitz, H., and Tullis, J.: Weakening and strain localization produced by syn-deformational reaction of plagioclase, *Int. J. Earth Sci.*, 90, 136–148, doi:10.1007/s005310000148, 2001.
- 30 Taylor, S. R. and McLennan, S. M.: *The Continental Crust: its Composition and Evolution*, Medium: X, Blackwell Scientific, Palo Alto, CA, USA, 328 pp., 1985.
- Treagus, S. H. and Treagus, J. E.: Studies of strain and rheology of conglomerates, *J. Struct. Geol.*, 24, 1541–1567, doi:10.1016/S0191-8141(01)00162-6, 2002.

Twiss, R. J. and Moores, E.: Structural Geology, edited by: Freeman, W. H., New York, USA, 1992.

Urai, J., Spaeth, G., van der Zee, W., and Hilgers, C.: Evolution of mullion (boudin) structures in the Variscan of the Ardennes and Eifel, Journal of the Virtual Explorer, 3, 1–16, 2001.

5 van der Molen, I.: Interlayer material transport during layer-normal shortening, Part II. Boudinage, pinch-and-swell and migmatite at Søndre Strømfjord Airport, West Greenland, Tectonophysics, 115, 297–313, doi:10.1016/0040-1951(85)90143-X, 1985.

10 Watts, M. J. and Williams, G. D.: Strain geometry, microstructure and mineral chemistry in metagabbro shear zones: a study of softening mechanisms during progressive mylonitization, J. Struct. Geol., 5, 507–517, doi:10.1016/0191-8141(83)90056-1, 1983.

Whitney, D. L. and Evans, B. W.: Abbreviations for names of rock-forming minerals, Am. Mineral., 95, 185, 2010.

Zulauf, J. and Zulauf, G.: Coeval folding and boudinage in four dimensions, J. Struct. Geol., 27, 1061–1068, doi:10.1016/j.jsrg.2005.04.003, 2005.

**SED**

7, 1517–1554, 2015

---

## **Pinch and swell structures**

R. Gardner et al.

---

Title Page

Abstract

Introduction

Conclusions

References

Tables

Figures

◀

▶

◀

▶

Back

Close

Full Screen / Esc

Printer-friendly Version

Interactive Discussion



## Pinch and swell structures

R. Gardner et al.

**Table 1.** Yielding and faulting parameters used for Mohr–Coulomb behaviour in the three layer model (see Moresi and Mühlhaus, 2006 and text for details).

Yielding parameter	Newtonian Flow	non_Newtonian Flow
Stress exponent ( $n$ )	1	3
Viscosity ratio ( $R_v$ ) <sup>a</sup>	10	10
Cohesion ratio ( $R_{Co}$ ) <sup>b</sup>	20	20
Friction coefficient ( $\mu$ )	0.6	0.6

<sup>a</sup>defined as  $R_v = \eta_{Bi}/\eta_{Ai}$  where  $\eta_{Bi}$  is the initial viscosity of the competent layer B and  $\eta_{Ai}$  is the initial viscosity of the matrix layers.

<sup>b</sup>defined as  $R_{Co} = c_i/c_s$  where  $c_i$  is the initial cohesion of the competent layer and  $c_s$  the cohesion after failure and softening.

[Title Page](#)
[Abstract](#)
[Introduction](#)
[Conclusions](#)
[References](#)
[Tables](#)
[Figures](#)
[Back](#)
[Close](#)
[Full Screen / Esc](#)
[Printer-friendly Version](#)
[Interactive Discussion](#)


## Pinch and swell structures

R. Gardner et al.

**Table 2.** Analysis III results showing effect of systematically varying Newtonian/non-Newtonian flow ( $n$  is stress exponent) and Mohr-Coulomb behaviour (M-CB) characteristics of the more competent layer B with respect to matrix layers (A) on pinch and swell development (detailed model results are provided in Fig. S2); an x indicates Mohr-Coulomb behaviour; P&S indicates pinch and swell structures formed in layer B for that simulation.

		(1)		(2)		(3)		(4)	
Layer: $n$		Matrix $n = 1$	Layer B $n = 1$	Matrix $n = 1$	Layer B $n = 3$	Matrix $n = 3$	Layer B $n = 1$	Matrix $n = 3$	Layer B $n = 3$
M-CB:	(i)	x	x P&S	x	x P&S	x	x P&S	x	x P&S
	(ii)	x		x		x		x	
	(iii)		x P&S		x P&S		x P&S		x P&S
	(iv)								

Title Page

Abstract

Introduction

Conclusions

References

Tables

Figures

I◀

▶I

◀

▶

Back

Close

Full Screen / Esc

Printer-friendly Version

Interactive Discussion



## Pinch and swell structures

R. Gardner et al.

Title Page

Abstract

Introduction

Conclusions

References

Tables

Figures

◀

▶

◀

▶

Back

Close

Full Screen / Esc

Printer-friendly Version

Interactive Discussion

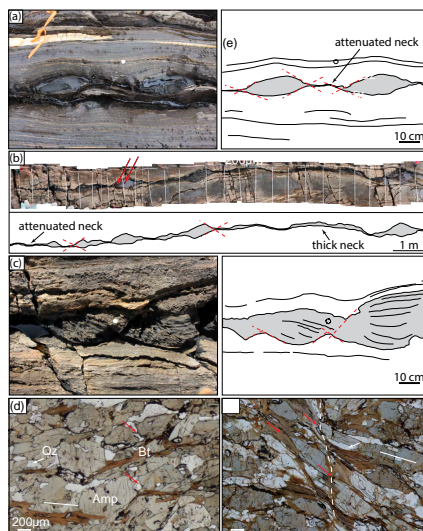


**Figure 1.** Pinch and swell structure characteristics, examples from the St. Anne Point rock platform, Fiordland, New Zealand ( $44^{\circ}34'19.9''$  S,  $167^{\circ}46'55.3''$  E). **(a) to (c)** Outcrop scale examples of pinch and swell structures; inferred positions of brittle failure shown as red dashed lines; **(a)** mafic layer showing pinch and swell structure with attenuated neck; **(b)** pinch and swell chain with attenuated and thick necks; red arrows show location of thin sections depicted in **(d)** and **(e)**; **(c)** pinch and swell structure in mafic layer showing brittle deformation and rotation of planar features; **(d)** and **(e)** brittle deformation at microscopic scale; plane polarised light; red arrows show sites of brittle deformation; minerals are labelled per Whitney and Evans (2010); white lines show foliation. Softer minerals biotite (Bt) and quartz (Qz) have filled brittle deformation localities. Modes of these softening minerals increases away from the swell centre. **(d)** The centre of swell (sample AS1331I); **(e)** the swell near the neck (sample AS1331G); asterisks indicate now separated pieces of a once continuous brittlely fractured amphibole grain; dashed white line shows inferred site for outcrop scale brittle fracture development.



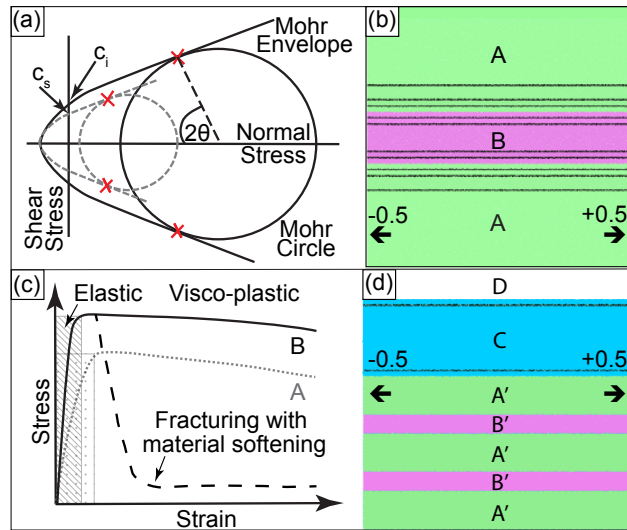


**Figure 2.** (a) Two examples of Mohr diagram showing theoretical cohesion value for two different materials as well as their faulting angle ( $\theta$ ) relationship, shown as black solid and grey dashed lines, red X signifies mode II failure;  $c_1$  and  $c_2$  is cohesion for material 1 and 2, difference in cohesion results in difference in shear stress value for the two materials. (b) Model set up for 3 layer model used in analysis tests I to IV; layer B more competent than matrix layers A, with passive marker beds (black lines) and constant velocity of  $-0.5$  on left and  $+0.5$  on the right. (c) Theoretical strain vs. stress diagram for elastic (cross-hatching and dots) and viscous flow (after Griggs and Handin, 1960); behaviour of layers A and B (with respect to 3 layer model (b)) are shown: competent layer B – solid line, less competent matrix layers A – dotted line; dashed line shows a layer with brittle deformation and material softening. (d) Multilayer crustal scale model used to explore effect of brittle behaviour on strain localisation and surface topography. The model includes an air layer (D) to allow realistic topographic feature development, an upper crust brittle layer (C) and 5 layers with two different material properties (layers A' and B') representing the middle to lower crust. Note: B' layers are more competent and A' layers.

## Pinch and swell structures

R. Gardner et al.

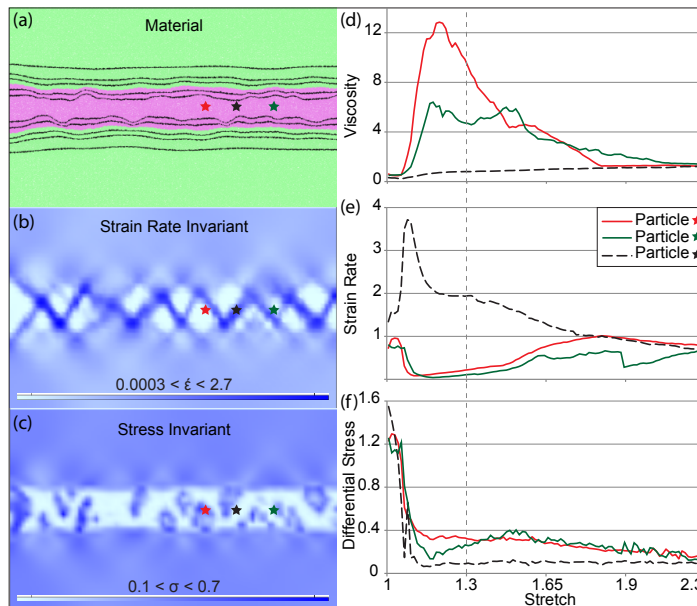


**Figure 3.** General model behaviour: snapshots (a–c) and graphs (d–f) showing characteristics of three sample particles from the  $n = 3$ ,  $R_V = 160$ , 3 layer model. Numerical results are shown for stretch 1.3 (grey dashed line on the graphs). Red and green stars indicate the location of two “tracer” particles in a low strain-high stress area which develops into a swell, while the black star indicates the location of a particle in the high strain-low stress area of the fracture which develops into a neck of the pinch and swell chain. Viscosity (d), strain rate (e) and differential stress (f) for these three particles are plotted against stretch. Note that the viscosity and strain rate graphs show an inverse relationship. See text for further explanation.

Title Page

Abstract

Introduction

Conclusions

References

Tables

Figures

◀

▶

◀

▶

Back

Close

Full Screen / Esc

Printer-friendly Version

Interactive Discussion



Pinch and swell structures

R. Gardner et al.

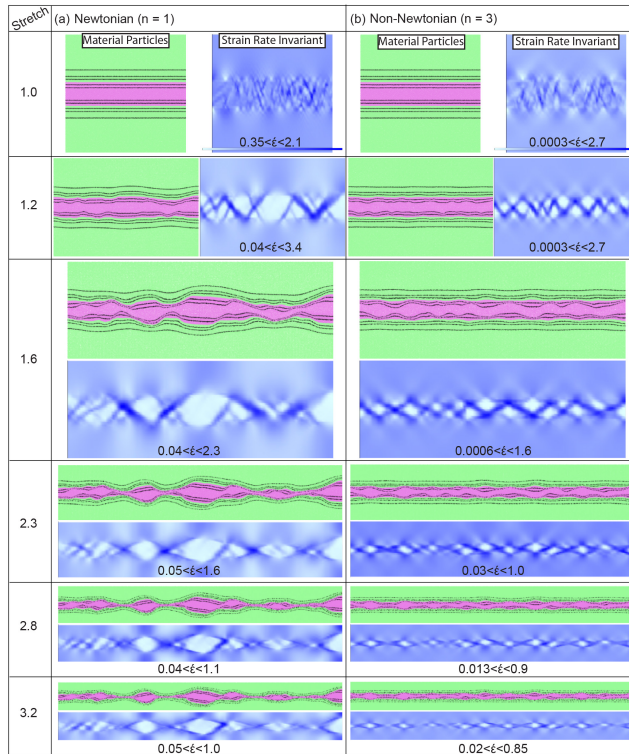


**Figure 4.** Analysis I results: series showing pinch and swell structure formation using the 3 layer model where layer B has Mohr–Coulomb brittle behaviour,  $R_V = 20$ ; **(a)** all layers have Newtonian flow ( $n = 1$ ) and **(b)** all layers have non-Newtonian flow ( $n = 3$ ). Pinch and swell structures successfully formed in Newtonian flow where strain is localised into a limited number of failure planes. Range of values is as specified while range of colour is the same for all model results showing strain rate invariant  $\dot{\epsilon}$ ; colour bars are included at stretch 1.0. Note: model results from stretch 1.6 have been zoomed to fit in the figure.

Title Page

Abstract

Introduction

Conclusions

References

Tables

Figures

◀

▶

◀

▶

Back

Close

Full Screen / Esc

Printer-friendly Version

Interactive Discussion



Pinch and swell structures

R. Gardner et al.

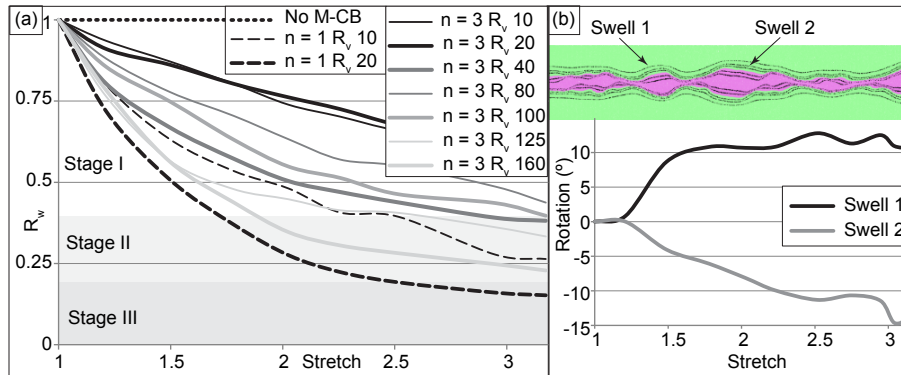


**Figure 5.** Analysis I and II results; **(a)** the effect of viscosity ratio ( $R_V$ ) in both Newtonian ( $n = 1$ ) and non-Newtonian ( $n = 3$ ) flow on pinch and swell structure formation in the 3 layer model.  $R_W$  is minimum neck width/maximum swell width at that stretch, where a low value indicates better pinch and swell development.  $R_W$  decreases as  $R_V$  increases indicating better pinch and swell development at higher  $R_V$  values. Pinch and swell structures are deemed to have initiated when  $R_W < 0.4$  and formed when  $R_W < 0.2$ . Three stages of pinch and swell growth are shown. **(b)** Rotation of passive marker beds can be either positive (swell 1) or negative (swell 2) as the model develops. Plotted data is from Newtonian ( $n = 1$ ) series in Fig. 4a.

Title Page

Abstract

Introduction

Conclusions

References

Tables

Figures



Back

Close

Full Screen / Esc

Printer-friendly Version

Interactive Discussion



## Pinch and swell structures

R. Gardner et al.

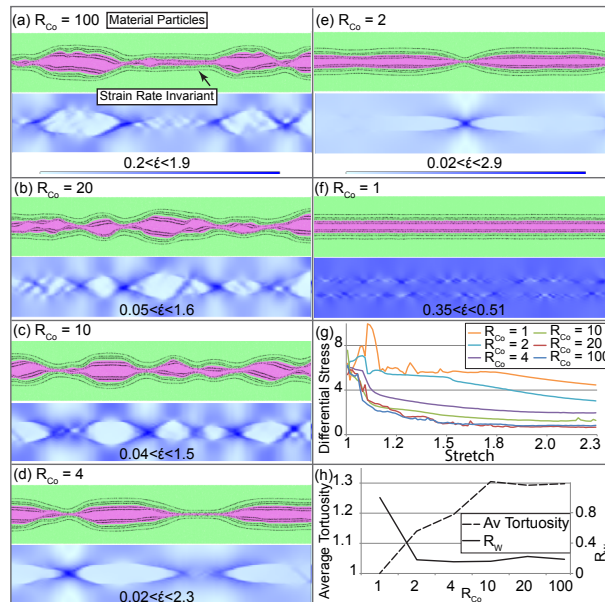


**Figure 6.** Analysis IV results: **(a–f)** model results at stretch 2.3 showing the effect of varying cohesion after softening in Newtonian flow with  $R_V = 10$ .  $R_{Co}$  is the ratio of initial cohesion to cohesion after softening (see text for definition); High  $R_{Co}$  **(a, b)** indicates strong material softening while  $R_{Co} = 1$  **(f)** has no material softening. Black arrow **(a)** shows formation of a thick neck. Strain rate invariant  $\dot{\epsilon}$  ranges of values are as specified while range of colour is the same for all images; colour bars are included on **(a)** and **(e)**. **(g)** Stretch vs. differential stress graph showing reduction in differential stress as material softening ( $R_{Co}$ ) is increased. Differential stress drops after fracturing and fluctuates until reaching a steady state depending on the  $R_{Co}$ . **(h)** Impact of  $R_{Co}$  on competent edge tortuosity and width ratio ( $R_W$ ) (see text for definitions). Tortuosity increases as  $R_{Co}$  increases to  $R_{Co} = 10$  reflecting more complex pinch and swell structures where  $R_{Co} > 10$ . Good pinch and swell structures are formed where  $R_{Co} > 2$  (i.e.  $R_W < 0.2$ ).

## Pinch and swell structures

R. Gardner et al.

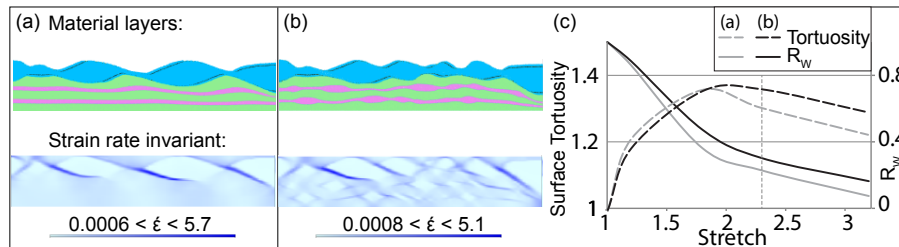


**Figure 7.** Multi-layer model results: non-Newtonian multi-layer models of the continental crust at stretch 2.3 showing differences in topography development (layer affinity results) and strain rate localisation (strain rate invariant results) where the mid to lower crust has viscosity difference (Layer B':Layer A' is  $R_v = 20$ ); **(a)** B' layers (pink) have no Mohr–Coulomb behaviour; **(b)** B' layers (pink) have initial brittle Mohr–Coulomb behaviour causing strain localisation through the whole model and more complex topography to develop. **(c)** Surface tortuosity (dashed lines) and  $R_w$  (solid lines) for the upper crustal (blue) layer from the models in **(a)** and **(b)**. At stretches  $> \sim 2$  model (a) has lower  $R_w$  (grey solid line) and lower surface tortuosity (grey dashed line) than model (b) reflecting the concentration of strain into the upper crust. Greater upper crust and surface complexity is seen where Mohr–Coulomb behaviour is included in the middle to lower crust (model b).

Title Page

Abstract

Introduction

Conclusions

References

Tables

Figures

◀

▶

◀

▶

Back

Close

Full Screen / Esc

Printer-friendly Version

Interactive Discussion

